L_0-Regularized Intensity and Gradient Prior for Text Images Deblurring and Beyond Supplemental Material

Jinshan Pan, Zhe Hu, Zhixun Su, and Ming-Hsuan Yang

1 Quantitative Evaluation on Text Image Dataset

In this section, we have created a dataset containing 15 images and 8 blur kernels extracted from Levin *et al.* [1]. Similar to [1], we can generate 120 different blurred images. The 15 ground truth images and 8 blur kernels are shown in Figures 1 and 2, respectively. For simplicity. we still use L0RIG and IL0RIG to denote the original text deblurring method [2] and the modified method for natural image deblurring.

(a) im01 (b) im02 (c) im03 (d) im04 (e) im05

(f) im06 (g) im07 (h) im08 (i) im09 (j) im10

(k) im11 (l) im12 (m) im13 (n) im14 (o) im15

Fig. 1. Ground truth text images.

For each image, we quantitatively compare average PSNRs among different methods [3], [4], [5], [6], [7], [8], [9] in Figure 3. The average PSNR values of all images are show in Table 1.

Figures 8 and 9 show some results from the test dataset.

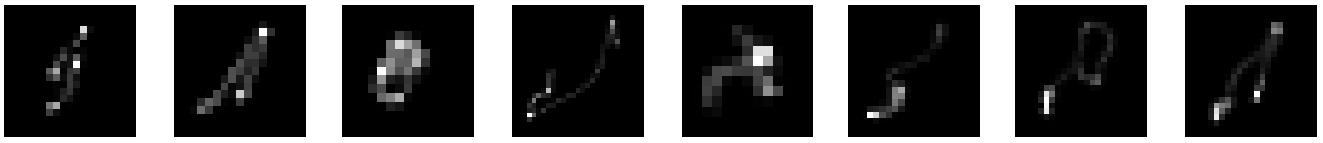

(a) kernel 1 (b) kernel 2 (c) kernel 3 (d) kernel 4 (e) kernel 5 (f) kernel 6 (g) kernel 7 (h) kernel 8

Fig. 2. Ground truth kernels.

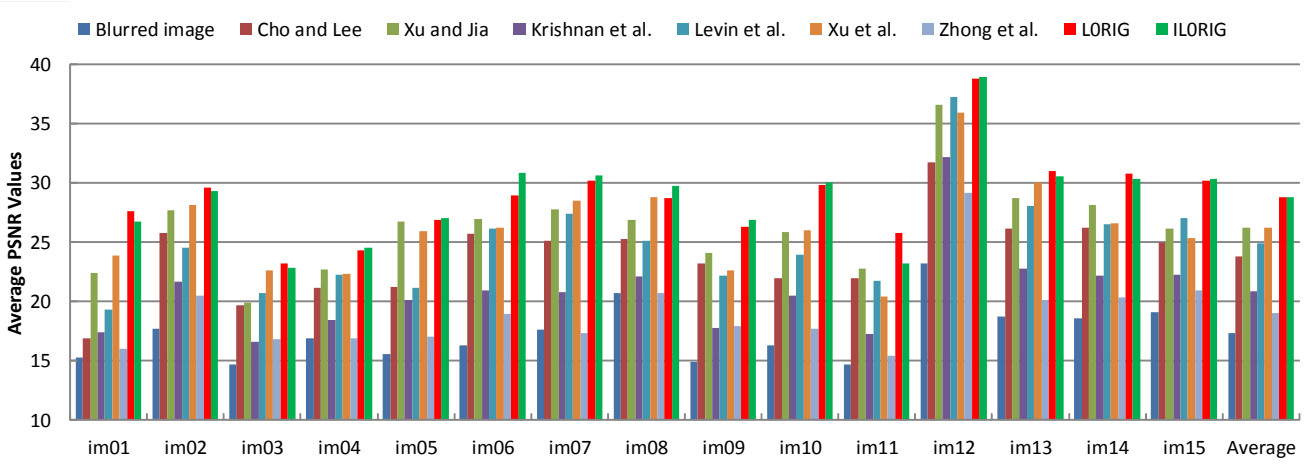

Fig. 3. Quantitative comparison on the dataset. The x-axis denotes the image index and the average PSNR values of all the images are shown on the rightmost column.

TABLE 1
The overall average PSNR values on text image dataset

	Blurred images	[4]	[5]	[6]	[7]	[8]	[9]	L0RIG	IL0RIG
Average PSNR	17.35	23.80	26.21	20.86	24.90	26.21	19.05	28.79	28.79

TABLE 2
The overall average PSNR values on low-illumination image dataset

	Blurred images	[4]	[5]	[6]	[8]	[11]	L0RIG	IL0RIG
Average PSNR	22.07	22.65	22.73	22.43	22.31	22.77	24.15	24.16

Since the code of Cho *et al.* [10] is not available, and the algorithm needs to adjust parameters to get the desirable results, we do not compare with [10] in this dataset. To make follow-up work easier, the MATLAB source code and above dataset will be made available to the public.

2 Quantitative Evaluation on Low-Illumination Image Dataset

In this section, we have created a dataset containing 6 low-illumination images and 8 blur kernels extracted from Levin *et al.* [1] (See Figure 2). Similar to [11], [12], we stretch the pixel intensities of each image into [0, 2.2] and then apply 8 different blur kernels. Finally we clip the pixel intensities into dynamic range [0, 1]. The 6 ground truth images are shown in Figure 6.

Figure 7 shows the average PSNR values of each image and Table 2 shows the overall PSNR values of this dataset.

3 Quantitative Evaluation on Natural Image Deblurring Datasets [1] and [13]

To verify the validity of the proposed method on the natural images, we test our method on the dataset [1], which contains 4 ground truth images and 8 blur kernels. Figure 10 (a) shows the cumulative histogram of the deconvolution error ratio across test examples. The proposed method achieves 100% of the results under error ratio 2.2 (See Table 3). Figure 11 shows one visual comparison from dataset [1]. Figures 12-15 show some visual comparisons from dataset [13].

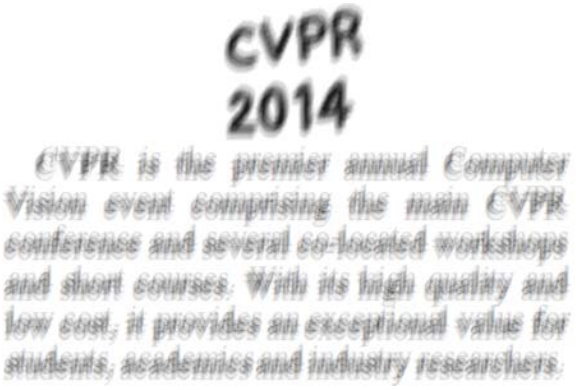

(a) Blurred image (PSNR: 14.74)

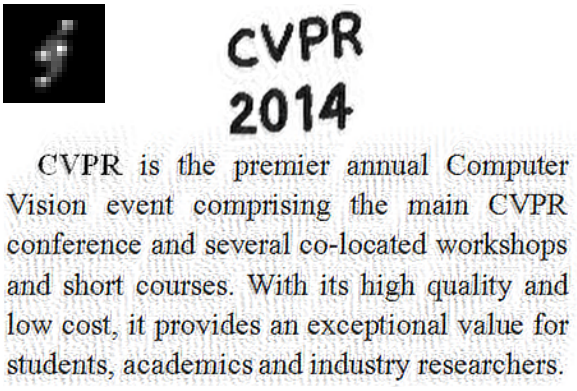

(b) Cho and Lee [4] (PSNR: 21.63)

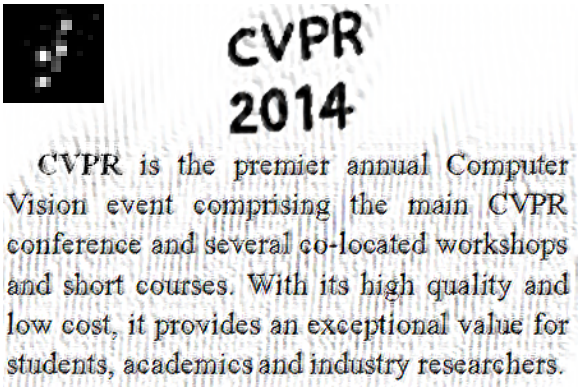

(c) Xu and Jia [5] (PSNR: 18.65)

(d) Krishnan *et al.* [6] (PSNR: 14.95)

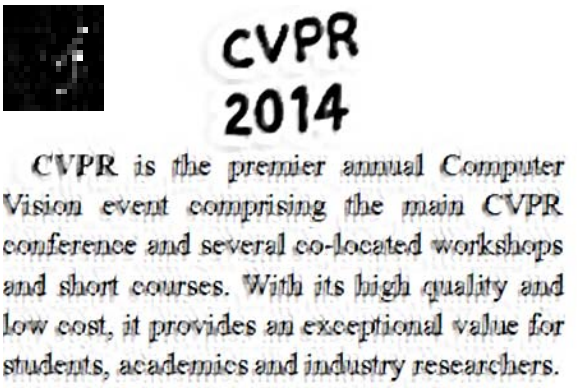

(e) Levin *et al.* [7] (PSNR: 17.67)

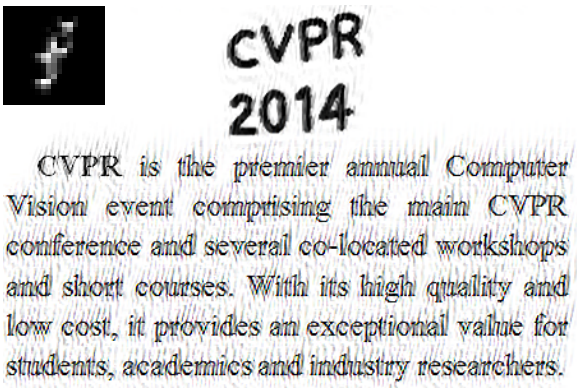

(f) Xu *et al.* [8] (PSNR: 17.46)

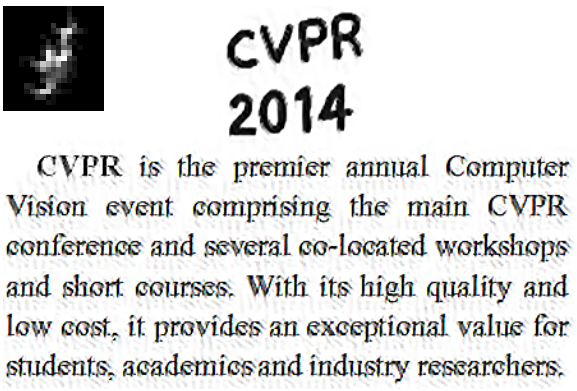

(g) L0RIG (PSNR: 18.95)

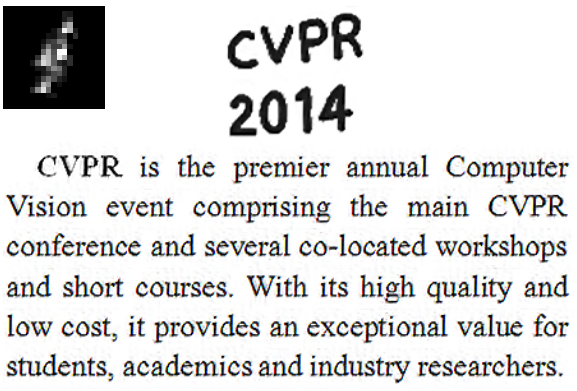

(h) IL0RIG (PSNR: 20.75)

Fig. 4. Visualization comparisons on the text image dataset.

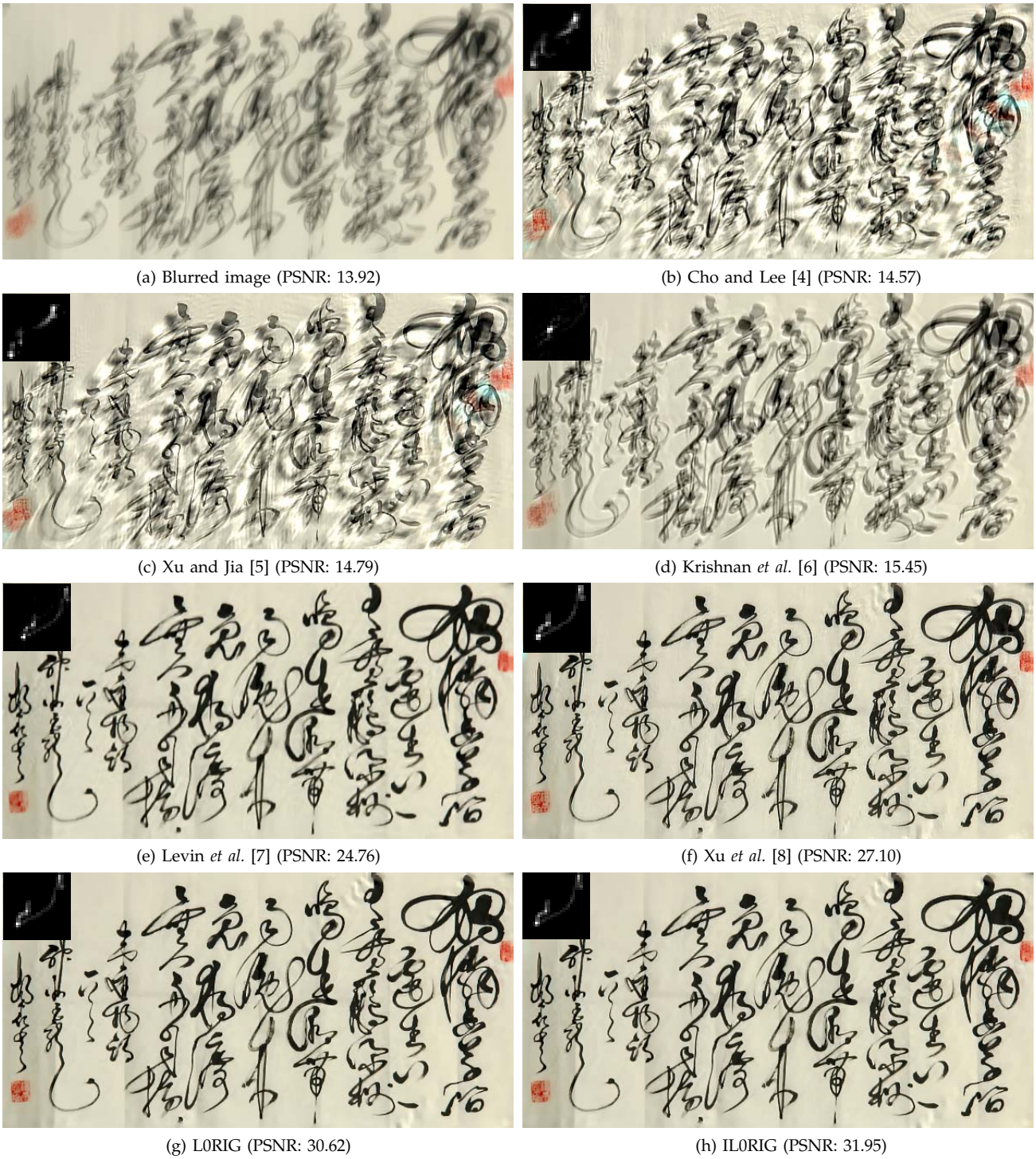

(a) Blurred image (PSNR: 13.92)

(b) Cho and Lee [4] (PSNR: 14.57)

(c) Xu and Jia [5] (PSNR: 14.79)

(d) Krishnan *et al.* [6] (PSNR: 15.45)

(e) Levin *et al.* [7] (PSNR: 24.76)

(f) Xu *et al.* [8] (PSNR: 27.10)

(g) L0RIG (PSNR: 30.62)

(h) IL0RIG (PSNR: 31.95)

Fig. 5. Visualization comparisons on the text image dataset.

(a) im01 (b) im02 (c) im03

(d) im04 (e) im05 (f) im06

Fig. 6. Ground truth low-illumination images.

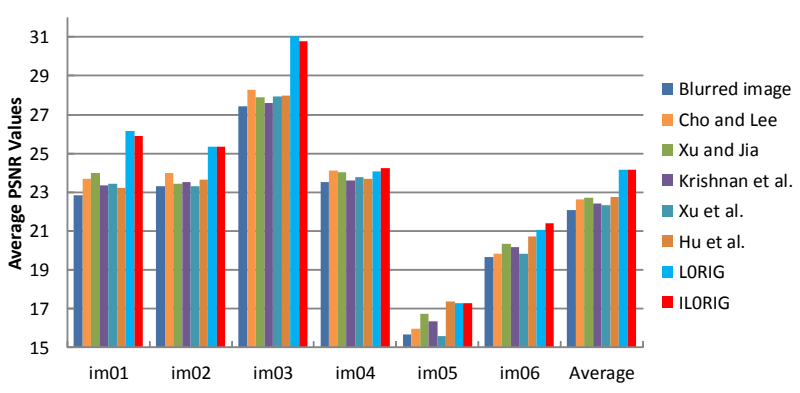

Fig. 7. Quantitative comparison on the low-illumination image dataset. The x-axis denotes the image index and the average PSNR values of all the images are shown on the rightmost column.

TABLE 3
The error ratio values of each restored image generated by IL0RIG on dataset [1]

	kernel 1	kernel 2	kernel 3	kernel 4	kernel 5	kernel 6	kernel 7	kernel 8
image 1	1.17	1.19	1.26	1.80	1.34	1.44	1.60	1.73
image 2	1.22	1.33	1.45	1.15	1.45	1.72	1.11	1.53
image 3	1.04	1.14	1.21	1.25	1.07	1.40	1.25	1.21
image 4	1.42	1.28	1.99	2.05	1.83	2.12	2.07	2.04

TABLE 4
The overall average PSNR values on natural image deblurring dataset [13]

	blurred image	[14]	[3]	[4]	[5]	[6]	[15]	[16]	L0RIG	IL0RIG
Average PSNR	24.93	2.73	25.89	28.98	29.54	25.73	26.84	28.07	28.40	29.65

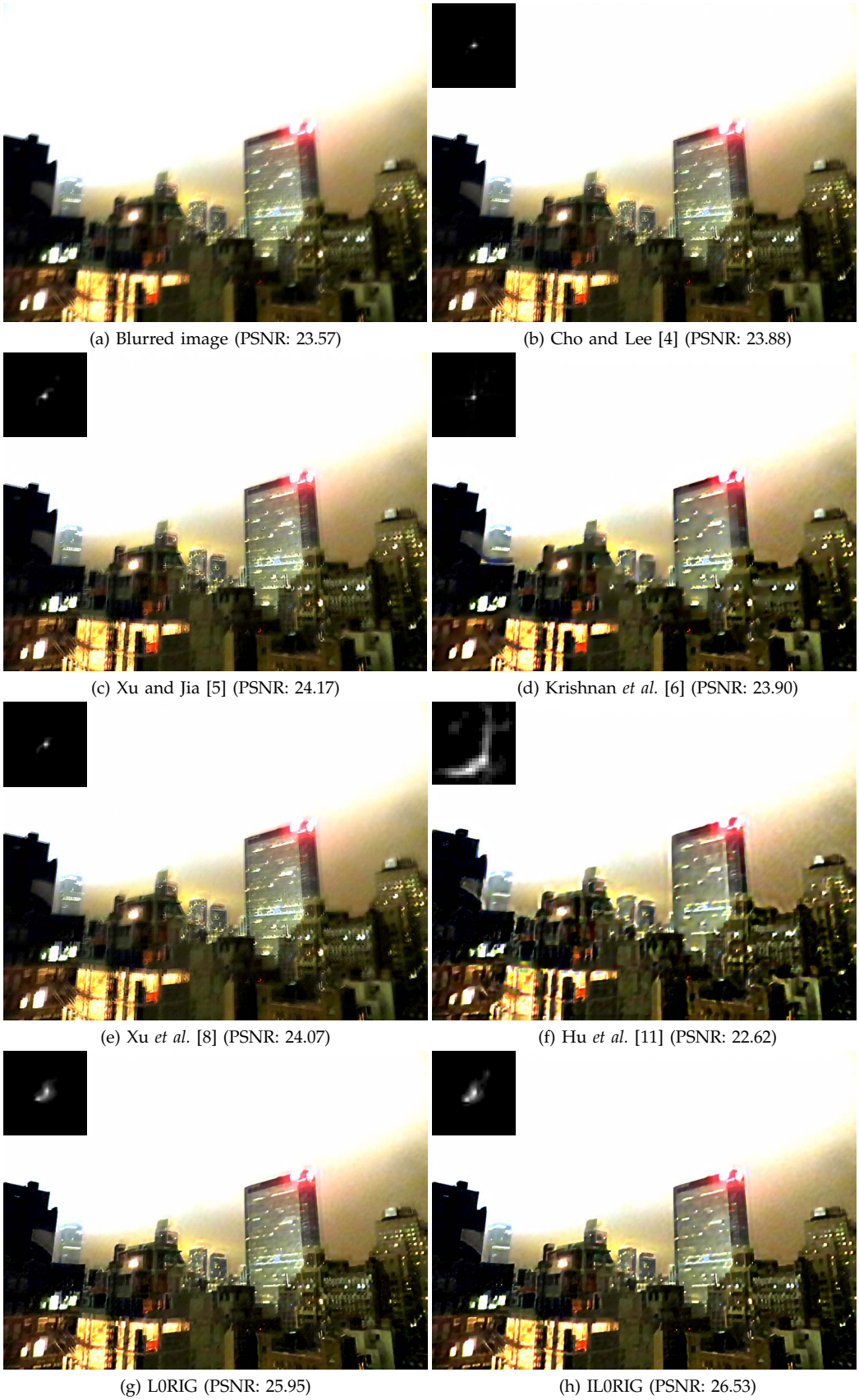

(a) Blurred image (PSNR: 23.57)
(b) Cho and Lee [4] (PSNR: 23.88)
(c) Xu and Jia [5] (PSNR: 24.17)
(d) Krishnan *et al.* [6] (PSNR: 23.90)
(e) Xu *et al.* [8] (PSNR: 24.07)
(f) Hu *et al.* [11] (PSNR: 22.62)
(g) L0RIG (PSNR: 25.95)
(h) IL0RIG (PSNR: 26.53)

Fig. 8. Visualization comparisons on the low-illumination image dataset.

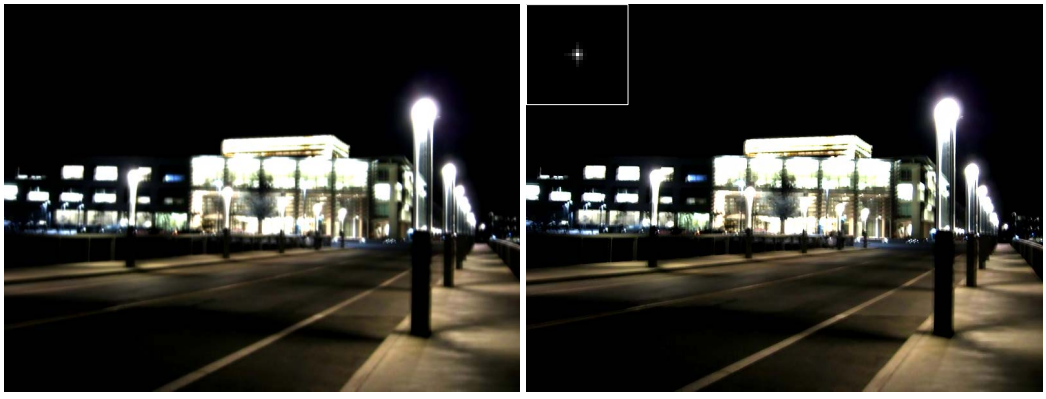

(a) Blurred image (PSNR: 22.68)

(b) Cho and Lee [4] (PSNR: 23.24)

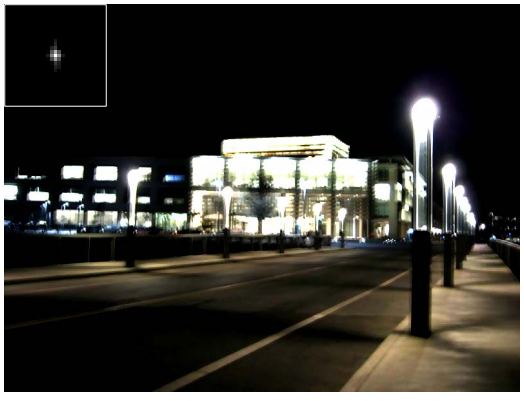

c) Xu and Jia [5] (PSNR: 23.43)

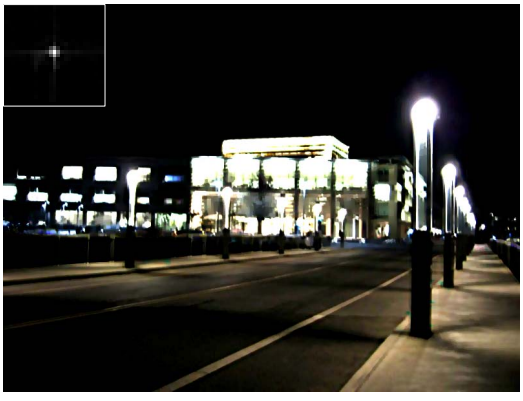

(d) Krishnan *et al.* [6] (PSNR: 23.72)

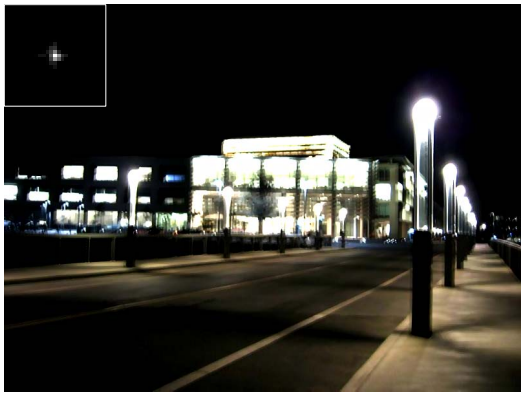

(e) Xu *et al.* [8] (PSNR: 23.26)

(f) Hu *et al.* [11] (PSNR: 21.48)

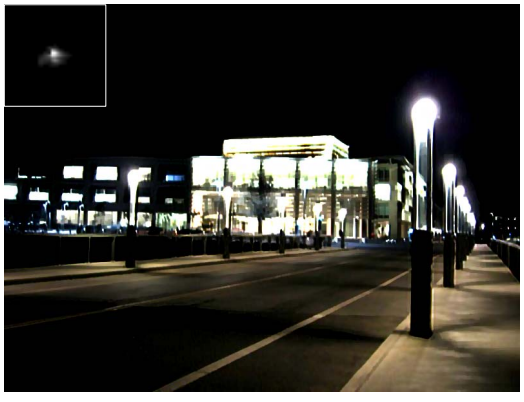

(g) L0RIG (PSNR: 24.75)

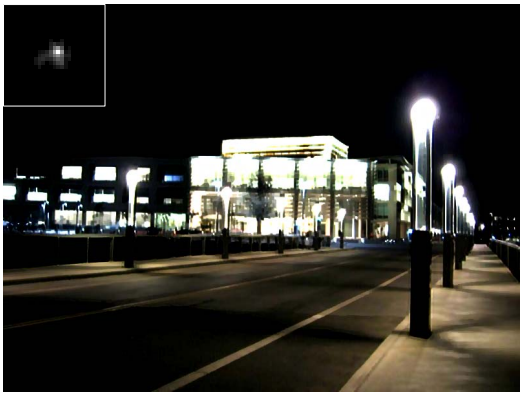

(h) IL0RIG (PSNR: 25.26)

Fig. 9. Visualization comparisons on the low-illumination image dataset.

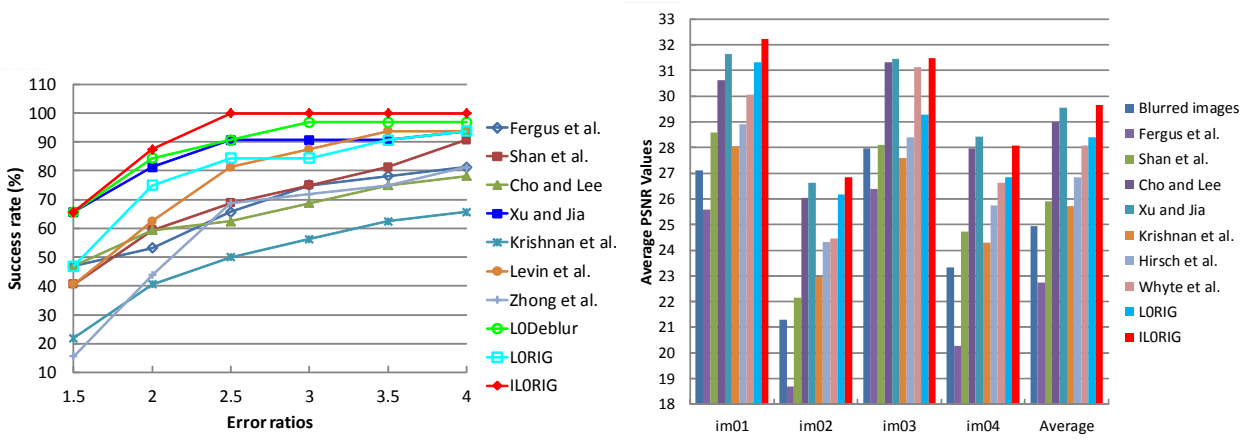

(a) Results on dataset [1] (b) Results on dataset [13]

Fig. 10. Quantitative comparison on the natural image datasets [1] and [13]. The numbers below the horizontal axis in (a) denote the error ratio values. Our method achieves 100% of the results under error ratio 2.2 on the dataset [1].

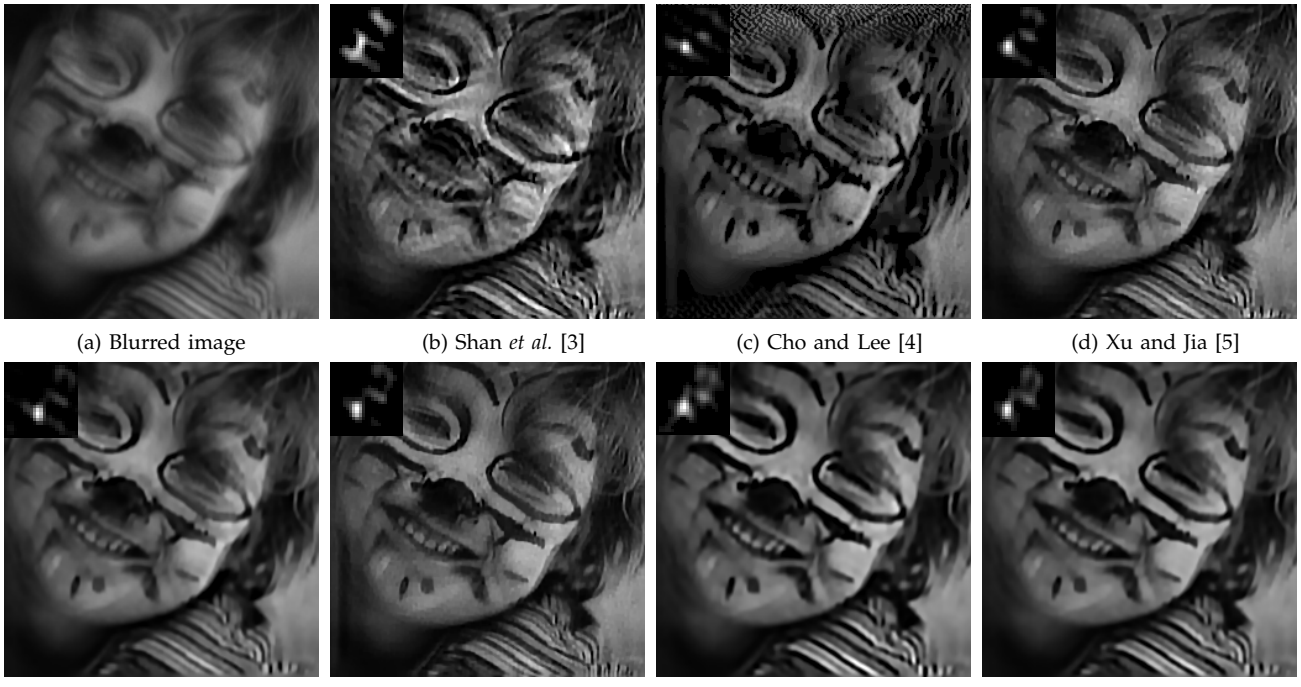

(a) Blurred image (b) Shan *et al.* [3] (c) Cho and Lee [4] (d) Xu and Jia [5]

(e) Levin *et al.* [7] (f) Xu *et al.* [8] (g) L0RIG (h) IL0RIG

Fig. 11. Visualization comparisons on the natural image dataset [1].

(a) Blurred image (b) Shan *et al.* [3] (c) Cho and Lee [4]

(d) Xu and Jia [5] (e) Krishnan *et al.* [6] (f) Hirsch *et al.* [15]

(g) Whyte *et al.* [16] (h) L0RIG (i) IL0RIG

Fig. 12. Visualization comparisons on the natural image dataset [1].

(a) Blurred image (b) Shan *et al.* [3] (c) Cho and Lee [4]

(d) Xu and Jia [5] (e) Krishnan *et al.* [6] (f) Hirsch *et al.* [15]

(g) Whyte *et al.* [16] (h) L0RIG (i) IL0RIG

Fig. 13. Visualization comparisons on the natural image dataset [1].

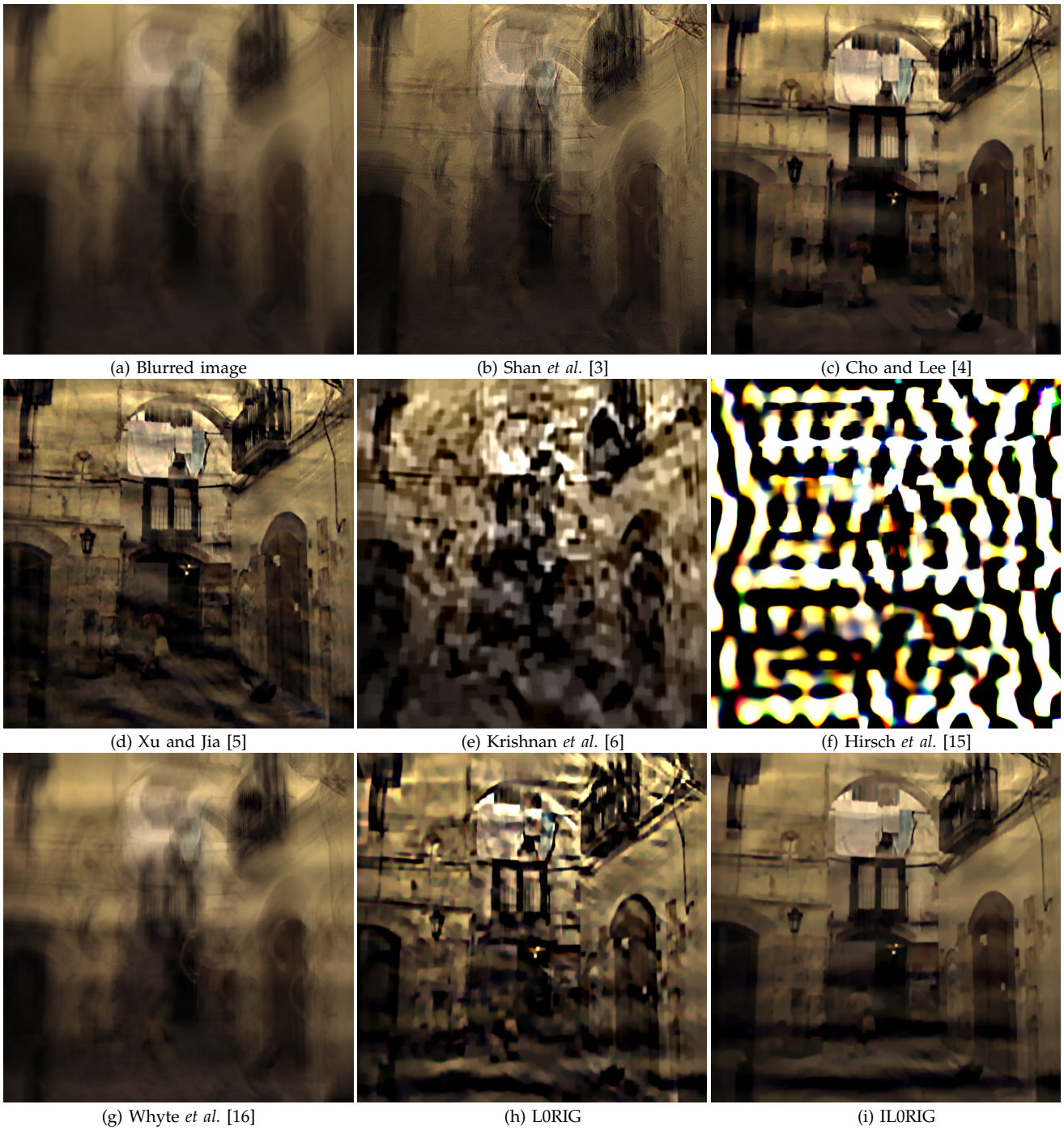

(a) Blurred image (b) Shan *et al.* [3] (c) Cho and Lee [4]

(d) Xu and Jia [5] (e) Krishnan *et al.* [6] (f) Hirsch *et al.* [15]

(g) Whyte *et al.* [16] (h) L0RIG (i) IL0RIG

Fig. 14. Visualization comparisons on the natural image dataset [1].

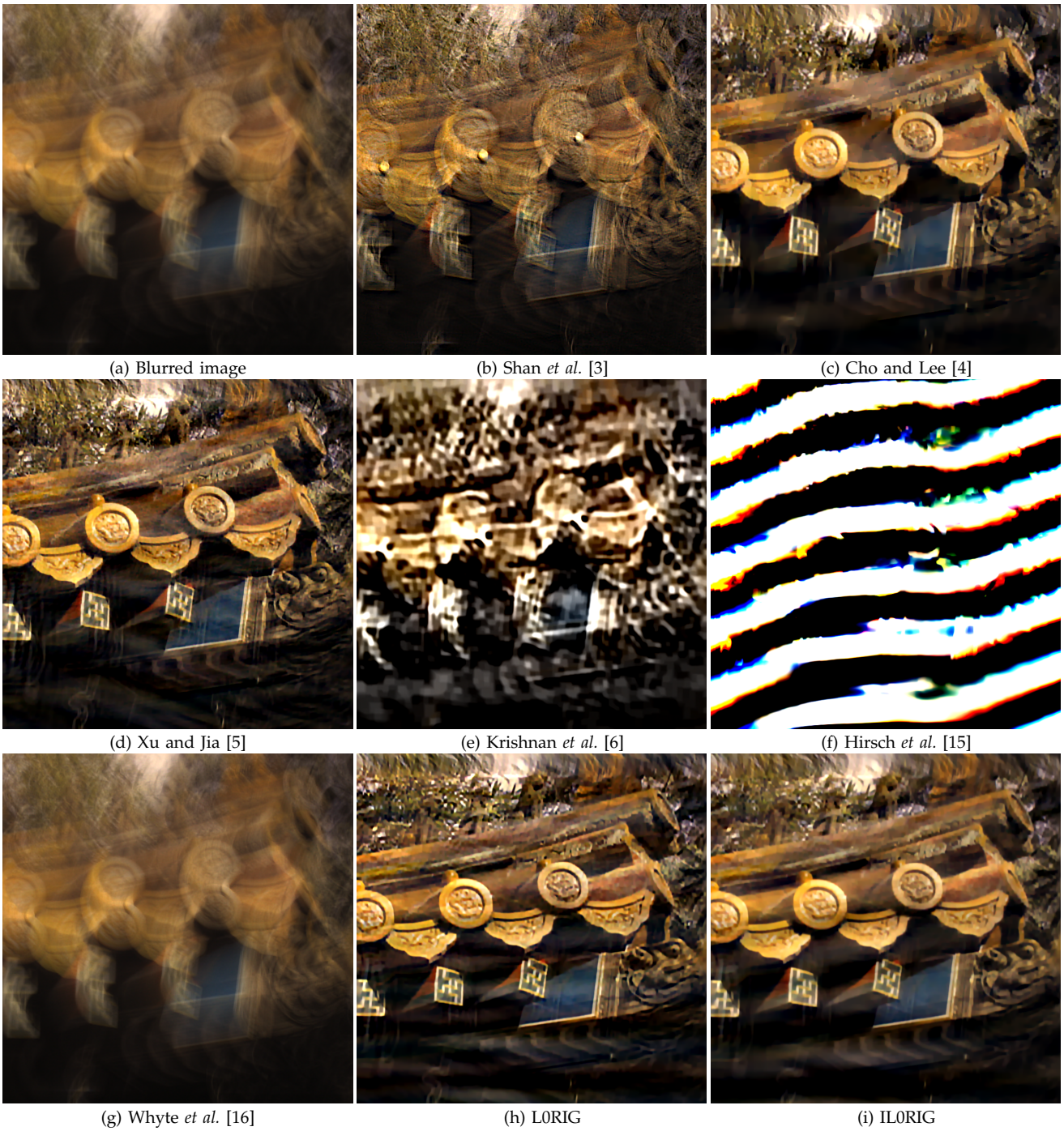

(a) Blurred image (b) Shan *et al.* [3] (c) Cho and Lee [4]

(d) Xu and Jia [5] (e) Krishnan *et al.* [6] (f) Hirsch *et al.* [15]

(g) Whyte *et al.* [16] (h) L0RIG (i) IL0RIG

Fig. 15. Visualization comparisons on the natural image dataset [1].

4 More Experimental Results

In this section, we show more comparison of results which do not appear in the manuscript. We compare our method with several state-of-the-art deblurring methods. It is noted that the codes or softwares of some state-of-the-art deblurring methods (*e.g.*, Levin *et al.* [7], Shan *et al.* [3]) do not generate the results due to the challenging blurred examples, so we do not compare these methods in some following figures.

4.1 Synthetic Blurred Text Images

(a) Blurred image and kernel (b) Cho and Lee [4] (PSNR: 7.03)

(c) Xu and Jia [5] (PSNR: 9.27) (d) Krishnan *et al.* [6] (PSNR: 8.16)

(e) Xu *et al.* [8] (PSNR: 8.20) (f) Cho *et al.* [10] (PSNR: 13.64)

(g) L0RIG (PSNR: 22.22) (h) IL0RIG (PSNR: 22.52)

Fig. 16. Synthetic example with large blur.

(a) Blurred image and kernel

(b) Shan *et al.* [3] (PSNR: 14.79)

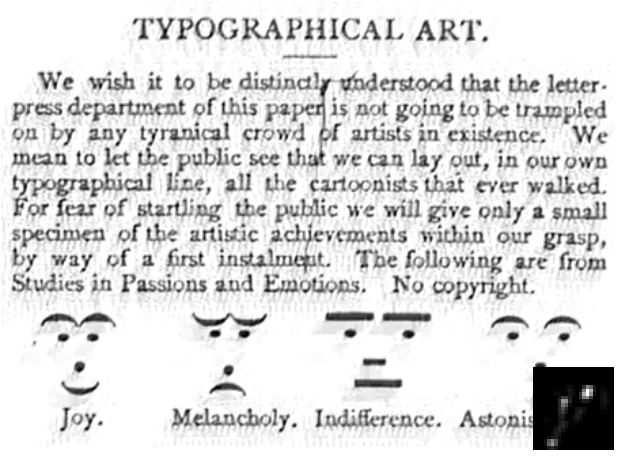

(c) Cho and Lee [4] (PSNR: 20.45)

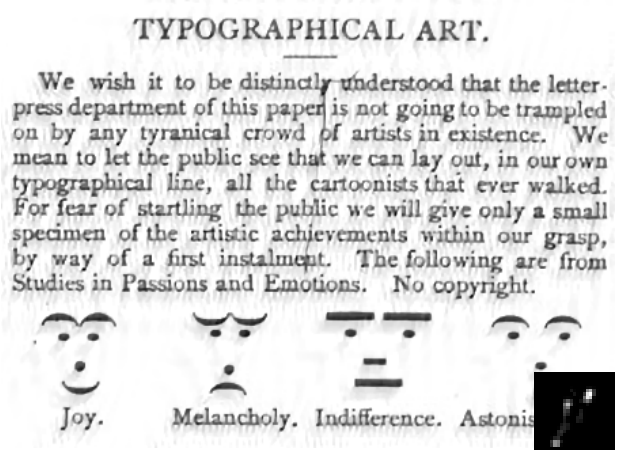

(d) Xu and Jia [5] (PSNR: 21.60)

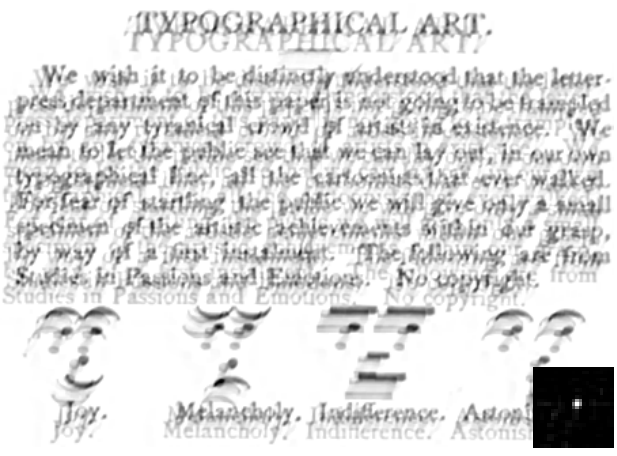

(e) Krishnan *et al.* [6] (PSNR: 15.83)

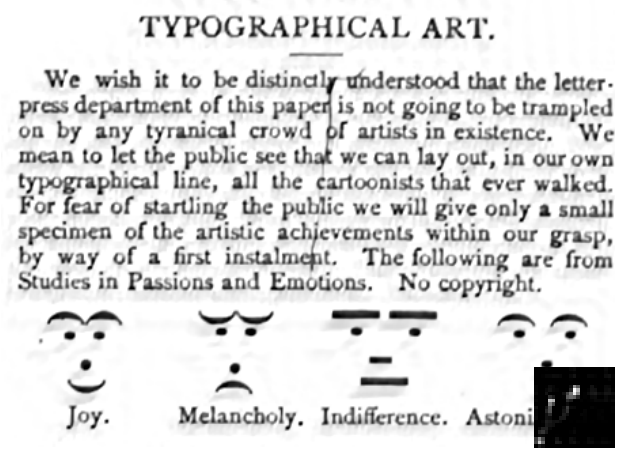

(f) Levin *et al.* [7] (PSNR: 19.43)

Fig. 17. A synthetic example from [10].

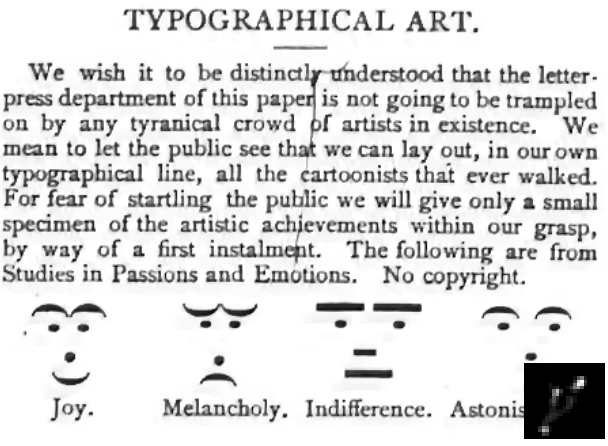

(g) Xu *et al.* [8] (PSNR: 24.21)

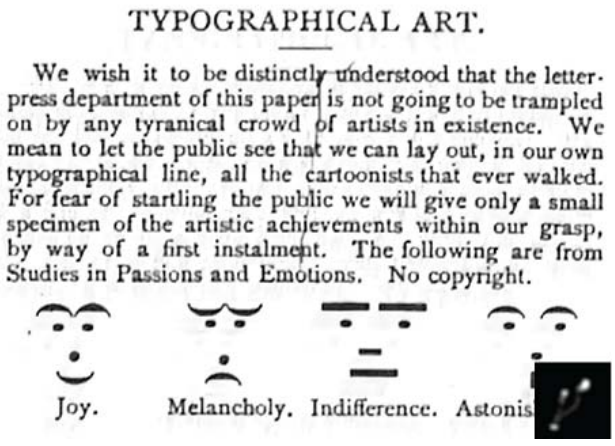

(h) Cho *et al.* [10] (PSNR: 23.96)

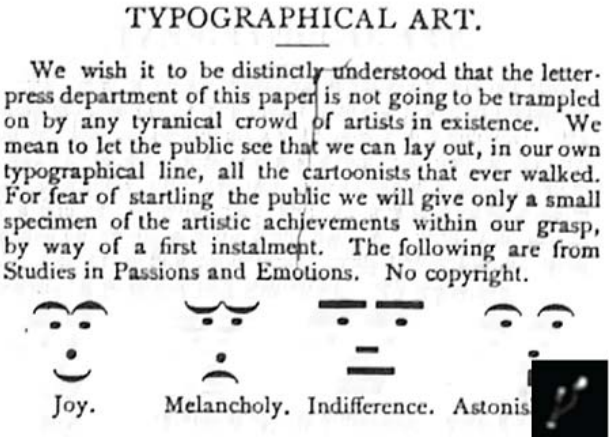

(i) L0RIG (PSNR: 27.08)

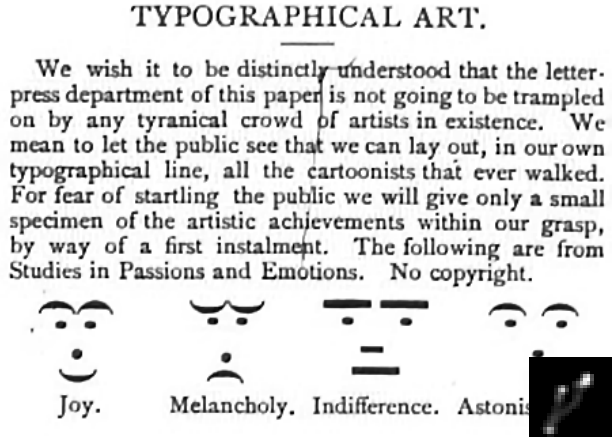

(j) IL0RIG (PSNR: 28.86)

Fig. 17. (**continued**) A synthetic example from [10].

4.2 Real Blurred Text Images

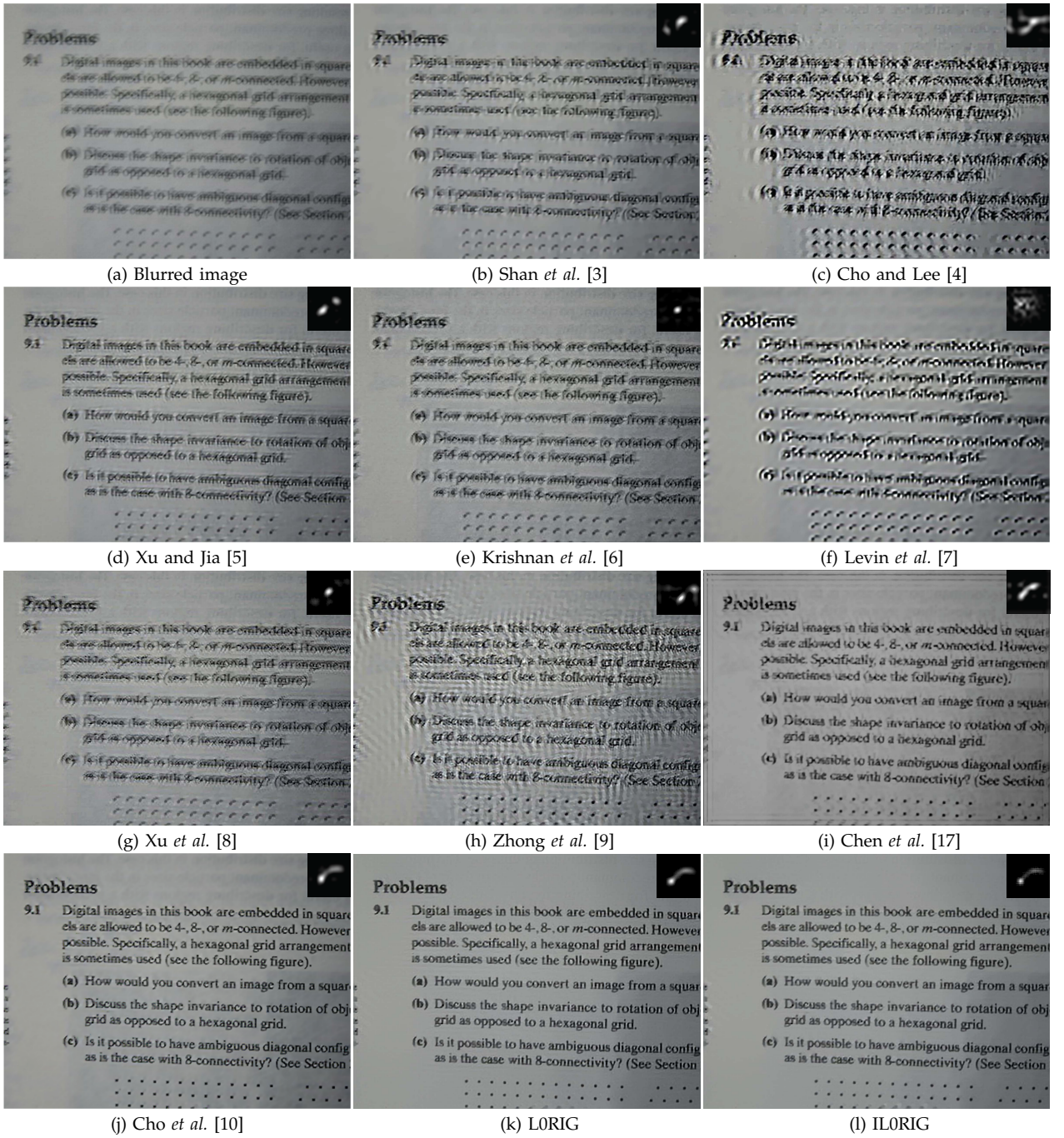

(a) Blurred image (b) Shan *et al.* [3] (c) Cho and Lee [4]

(d) Xu and Jia [5] (e) Krishnan *et al.* [6] (f) Levin *et al.* [7]

(g) Xu *et al.* [8] (h) Zhong *et al.* [9] (i) Chen *et al.* [17]

(j) Cho *et al.* [10] (k) L0RIG (l) IL0RIG

Fig. 18. Real captured example. Our method generates the better deblurred result with less ringing artifacts compared to [10].

4.3 Natural Blurred Images with Severe Saturated Areas

In this section, we use some real captured blurred images with severe saturated areas to verify the validity of the proposed kernel estimation method.

4.4 Natural Image Deblurring

We compare our method with the state-of-the-art natural image deblurring methods [14], [4], [5], [8] by using the images that are presented in their manuscripts.

4.5 Non-Uniform Image Deblurring

In this section, we show comparison results of the non-uniform deblurring methods.

REFERENCES

[1] A. Levin, Y. Weiss, F. Durand, and W. T. Freeman, "Understanding and evaluating blind deconvolution algorithms," in *CVPR*, 2009, pp. 1964–1971.
[2] J. Pan, Z. Hu, Z. Su, and M.-H. Yang, "Deblurring text images via L_0-regularized intensity and gradient prior," in *CVPR*, 2014, pp. 2901–2908.
[3] Q. Shan, J. Jia, and A. Agarwala, "High-quality motion deblurring from a single image," *ACM Transactions on Graphics*, vol. 27, no. 3, p. 73, 2008.
[4] S. Cho and S. Lee, "Fast motion deblurring," *ACM Transactions on Graphics*, vol. 28, no. 5, p. 145, 2009.
[5] L. Xu and J. Jia, "Two-phase kernel estimation for robust motion deblurring," in *ECCV*, 2010, pp. 157–170.
[6] D. Krishnan, T. Tay, and R. Fergus, "Blind deconvolution using a normalized sparsity measure," in *CVPR*, 2011, pp. 2657–2664.
[7] A. Levin, Y. Weiss, F. Durand, and W. T. Freeman, "Efficient marginal likelihood optimization in blind deconvolution," in *CVPR*, 2011, pp. 2657–2664.
[8] L. Xu, S. Zheng, and J. Jia, "Unnatural l_0 sparse representation for natural image deblurring," in *CVPR*, 2013, pp. 1107–1114.
[9] L. Zhong, S. Cho, D. Metaxas, S. Paris, and J. Wang, "Handling noise in single image deblurring using directional filters," in *CVPR*, 2013, pp. 612–619.
[10] H. Cho, J. Wang, and S. Lee, "Text image deblurring using text-specific properties," in *ECCV*, 2012, pp. 524–537.
[11] Z. Hu, S. Cho, J. Wang, and M.-H. Yang, "Deblurring low-light images with light streaks," in *CVPR*, 2014, pp. 3382–3389.
[12] S. Cho, J. Wang, and S. Lee, "Handling outliers in non-blind image deconvolution," in *ICCV*, 2011, pp. 495–502.
[13] R. Köhler, M. Hirsch, B. J. Mohler, B. Schölkopf, and S. Harmeling, "Recording and playback of camera shake: Benchmarking blind deconvolution with a real-world database," in *ECCV*, 2012, pp. 27–40.
[14] R. Fergus, B. Singh, A. Hertzmann, S. T. Roweis, and W. T. Freeman, "Removing camera shake from a single photograph," *ACM Transactions on Graphics*, vol. 25, no. 3, pp. 787–794, 2006.
[15] M. Hirsch, C. J. Schuler, S. Harmeling, and B. Schölkopf, "Fast removal of non-uniform camera shake," in *ICCV*, 2011, pp. 463–470.
[16] O. Whyte, J. Sivic, A. Zisserman, and J. Ponce, "Non-uniform deblurring for shaken images," *International Jouunal on Computer Vision*, vol. 98, no. 2, pp. 168–186, 2012.
[17] X. Chen, X. He, J. Yang, and Q. Wu, "An effective document image deblurring algorithm," in *CVPR*, 2011, pp. 369–376.
[18] O. Whyte, J. Sivic, and A. Zisserman, "Deblurring shaken and partially saturated images," in *ICCV Workshops*, 2011, pp. 745–752.
[19] A. Gupta, N. Joshi, C. L. Zitnick, M. F. Cohen, and B. Curless, "Single image deblurring using motion density functions." in *ECCV*, 2010, pp. 171–184.
[20] Z. Hu and M. Yang, "Fast non-uniform deblurring using constrained camera pose subspace," in *BMVC*, 2012, pp. 1–11.

(a) Blurred image (b) Fergus *et al.* [14] (c) Shan *et al.* [3]

(d) Cho and Lee [4] (e) Xu and Jia [5] (f) Krishnan *et al.* [6]

(g) Levin *et al.* [7] (h) Xu *et al.* [8] (i) Zhong *et al.* [9]

(j) Cho *et al.* [10] (k) L0RIG (l) IL0RIG

Fig. 19. Real captured example. Our method generates the better deblurred result with less ringing artifacts compared to [10].

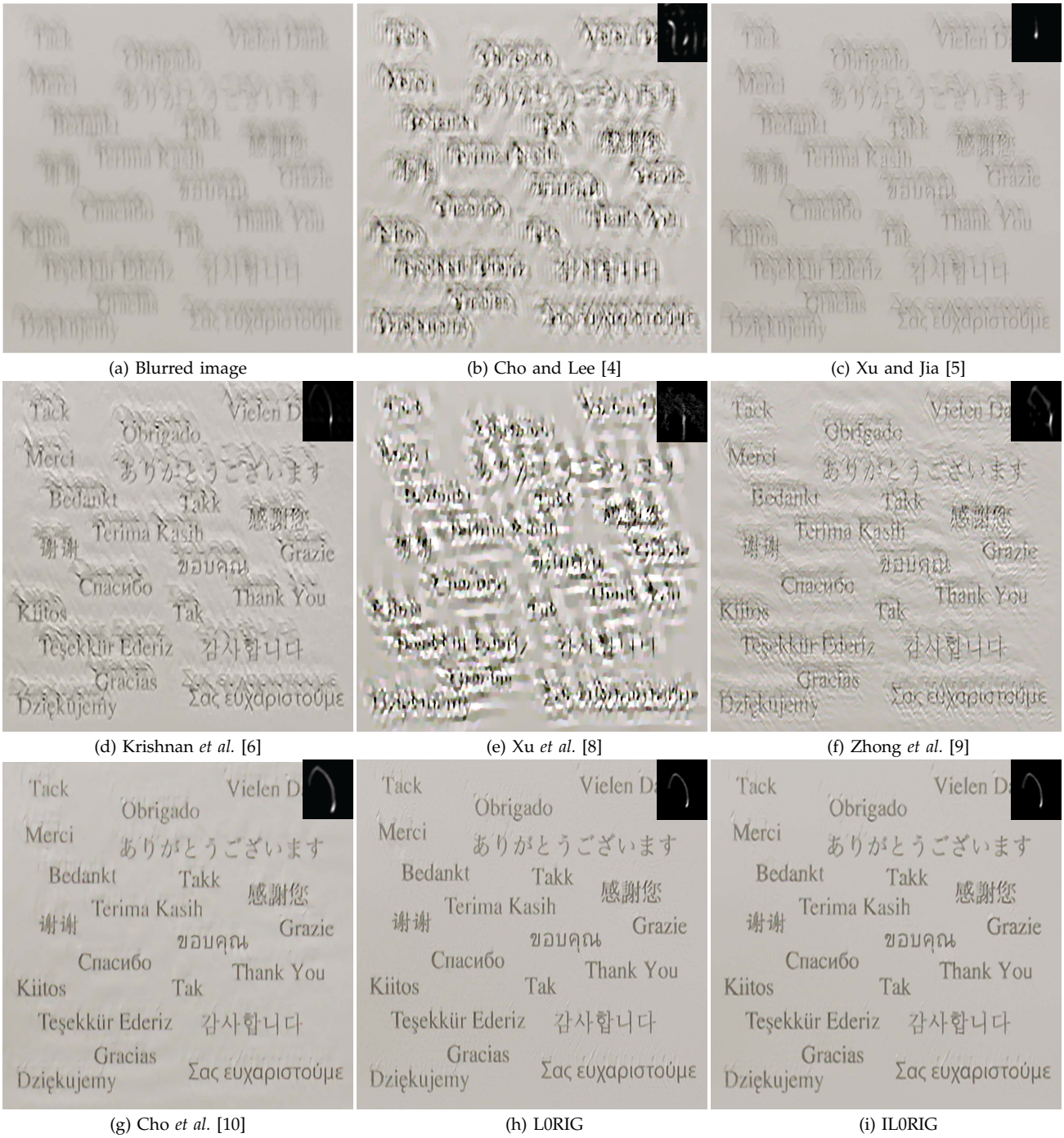

(a) Blurred image (b) Cho and Lee [4] (c) Xu and Jia [5]

(d) Krishnan *et al.* [6] (e) Xu *et al.* [8] (f) Zhong *et al.* [9]

(g) Cho *et al.* [10] (h) L0RIG (i) IL0RIG

Fig. 20. Real captured example. Our method generates the better deblurred result with less ringing artifacts compared to [10].

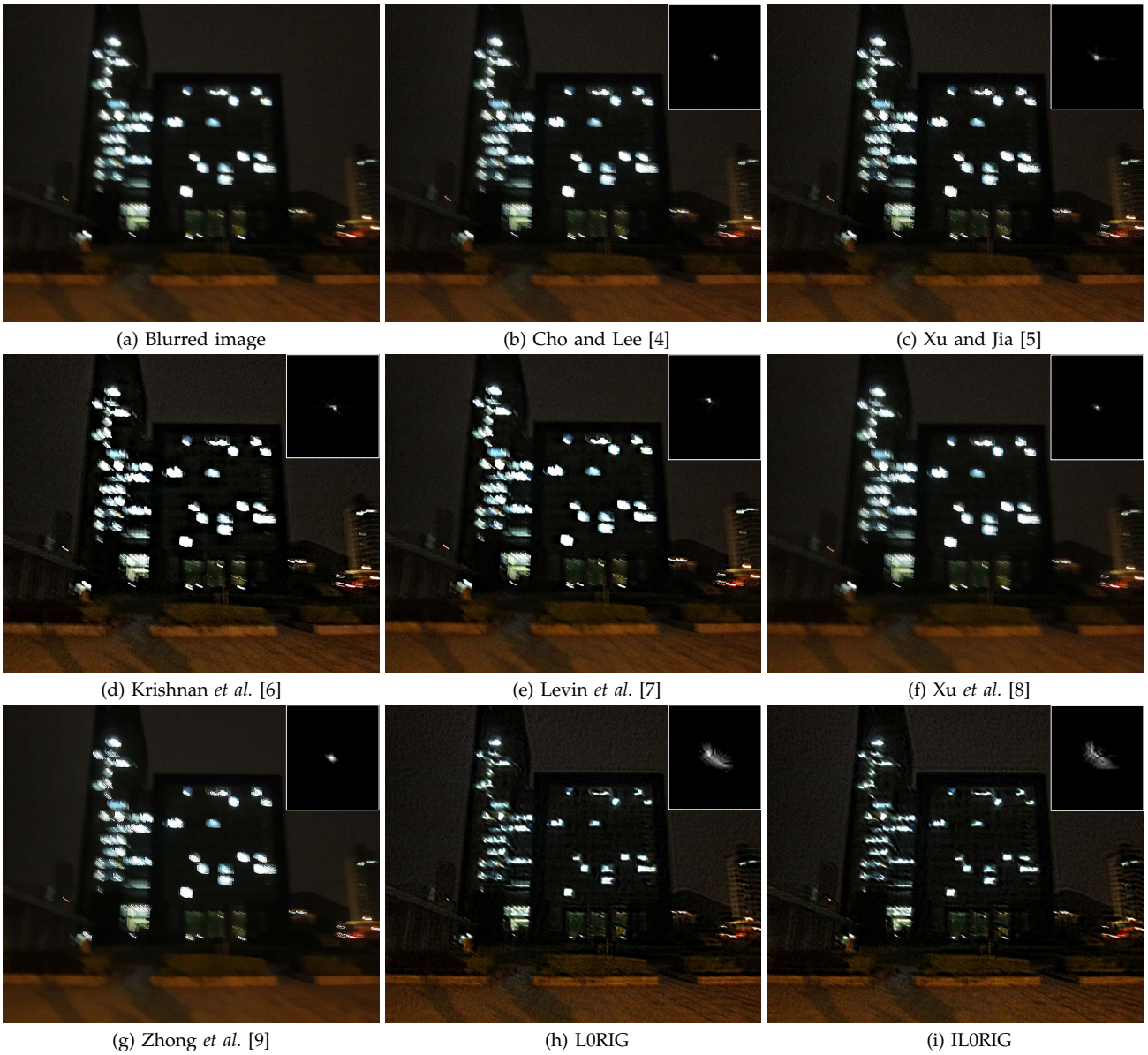

(a) Blurred image (b) Cho and Lee [4] (c) Xu and Jia [5]

(d) Krishnan *et al.* [6] (e) Levin *et al.* [7] (f) Xu *et al.* [8]

(g) Zhong *et al.* [9] (h) L0RIG (i) IL0RIG

Fig. 21. Real captured example containing lots of saturated areas. The kernel estimates of [4], [5], [6], [7], [8], [9] look like delta kernels. Our method generates a better kernel estimate.

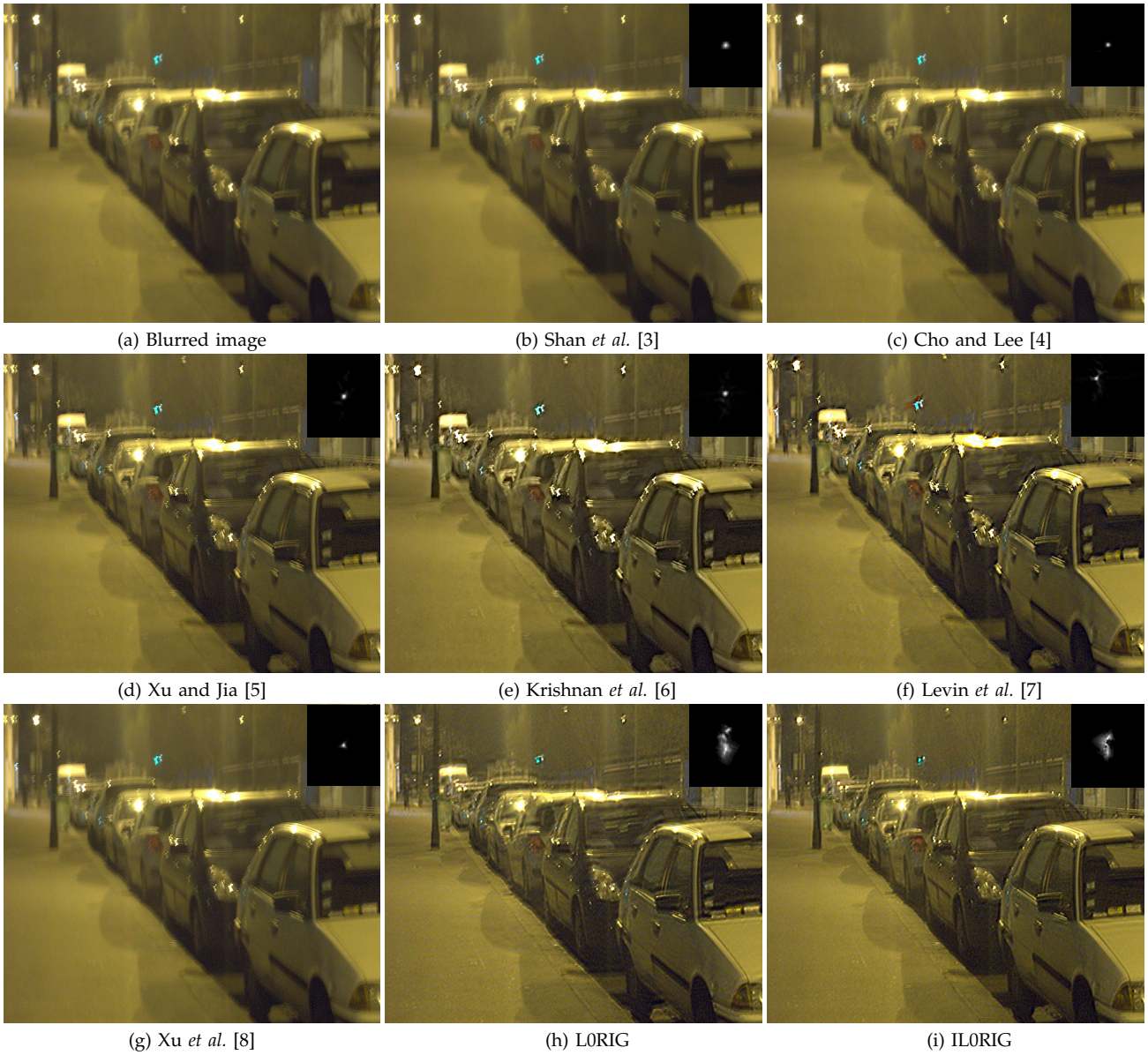

(a) Blurred image (b) Shan *et al.* [3] (c) Cho and Lee [4]

(d) Xu and Jia [5] (e) Krishnan *et al.* [6] (f) Levin *et al.* [7]

(g) Xu *et al.* [8] (h) L0RIG (i) IL0RIG

Fig. 22. Real captured example containing lots of saturated areas. The kernel estimates of [3], [4], [5], [6], [7], [8], [9] look like delta kernels. Our method generates a better kernel estimate. This image is obtained from [18].

(a) Blurred image (b) Cho and Lee [4] (c) Xu and Jia [5]

(d) Krishnan *et al.* [6] (e) Levin *et al.* [7] (f) Xu *et al.* [8]

(g) Hu *et al.* [11] (h) L0RIG (i) IL0RIG

Fig. 23. An example containing lots of saturated areas. Our method generates comparable results compared to [11] which mainly focuses on blurred images with low-light streaks.

(a) Blurred image (b) Fergus *et al.* [14] (c) IL0RIG

(a) Blurred image (b) Cho and Lee [4] (c) IL0RIG

(a) Blurred image (b) Xu and Jia [5] (c) IL0RIG

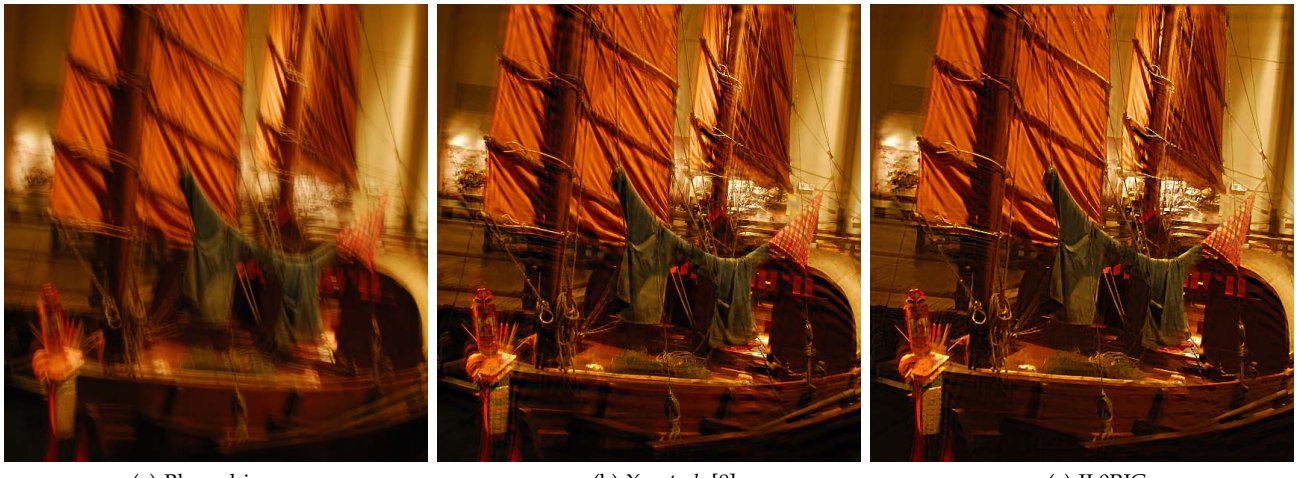

(a) Blurred image (b) Xu *et al.* [8] (c) IL0RIG

Fig. 24. Natural image deblurring examples. Our method generates comparable or even better results compared to the state-of-the-art natural image deblurring methods.

(a) Blurred image (b) Cho and Lee [4]

(c) Gupta *et al.* [19] (d) Whyte *et al.* [16]

(e) Xu *et al.* [8] (f) IL0RIG

Fig. 25. Comparison of non-uniform deblurred results. Our method generates a results with clearer characters (the enclosed part in green box in (f)). (best viewed on high-resolution display)

(a) Blurred image (b) Cho and Lee [4]

(c) Hrisch *et al.* [15] (d) Hu and Yang [20]

(e) Xu *et al.* [8] (f) IL0RIG

Fig. 26. Comparison of non-uniform deblurred results. Our method generates a results with clearer characters (the enclosed part in red box in (f)). (best viewed on high-resolution display)

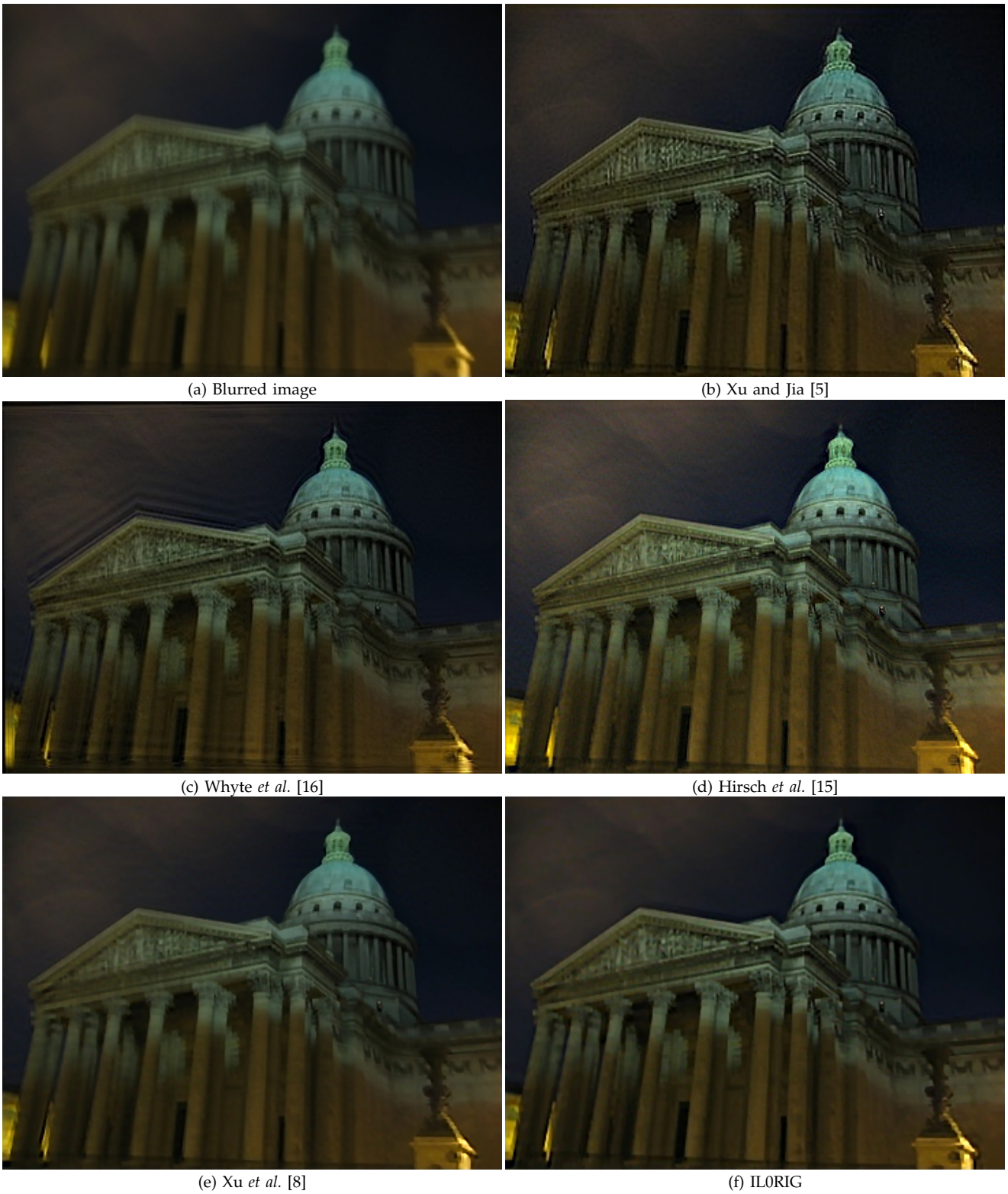

(a) Blurred image (b) Xu and Jia [5]

(c) Whyte *et al.* [16] (d) Hirsch *et al.* [15]

(e) Xu *et al.* [8] (f) IL0RIG

Fig. 27. Comparison of non-uniform deblurred results. The results shown in (b)-(c) contain some ringing artifacts and the result in (e) contains some blur (best viewed on high-resolution display).

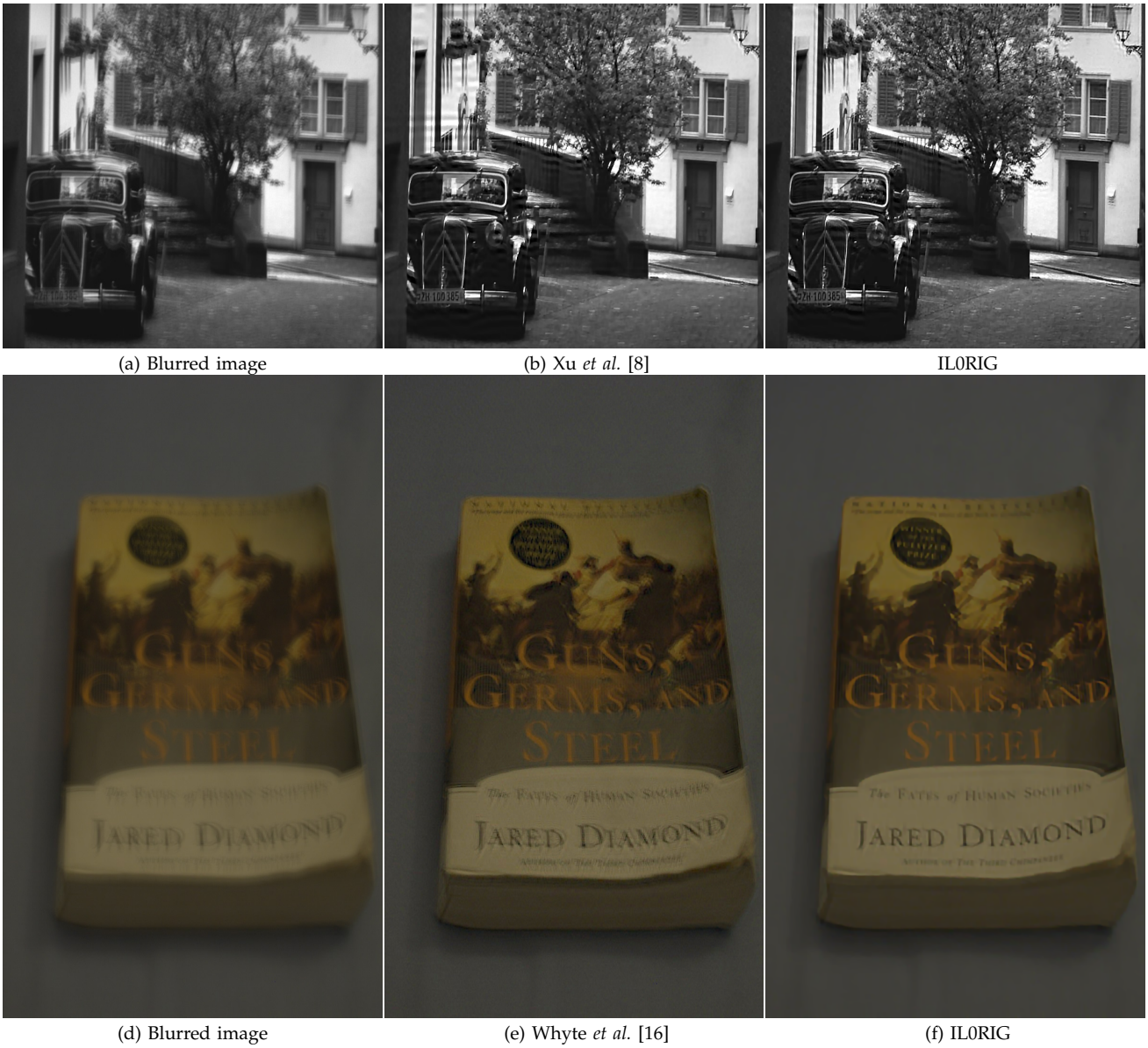

(a) Blurred image (b) Xu *et al.* [8] IL0RIG

(d) Blurred image (e) Whyte *et al.* [16] (f) IL0RIG

Fig. 28. Comparison of non-uniform deblurred results. Our method generates a results with few ringing artifacts (best viewed on high-resolution display).